

Article

Sediment Bed Borehole Advection Method

Scott Augustine ¹, Jaehyun Cho ¹, Harald Klammler ² , Kirk Hatfield ³ and Michael D. Annable ^{1,*} 

¹ Department of Environmental Engineering Sciences, University of Florida, Gainesville, FL 32611, USA; scott67@ufl.edu (S.A.); jaehyun.cho@essie.ufl.edu (J.C.)

² Department of Geosciences, Federal University of Bahia, Salvador 40170-290, Bahia, Brazil; haki@ufl.edu

³ Engineering School of Sustainable Infrastruct & Environment, University of Florida, Gainesville, FL 32611, USA; kirk.hatfield@essie.ufl.edu

* Correspondence: annable@ufl.edu; Tel.: +1-352-392-3294

Received: 29 October 2020; Accepted: 26 November 2020; Published: 2 December 2020



Abstract: This paper introduces and tests the Sediment Bed Borehole Advection Method (SBBAM), a low cost, point-measurement technique which utilizes a push-point probe to quantify the vertical direction and magnitude of Darcy flux at the surface water—groundwater sediment interface. The Darcy flux measurements are derived from the residence-time analysis of tracer arrival calculated from measured tracer concentration time-series data. The technique was evaluated in the laboratory using a sediment bed simulator tank at eight flow rates (1–90 cm/day). Triplicate test runs for each flow rate returned average errors between 4–20 percent; $r^2 = 0.9977$.

Keywords: Darcy flux; temporal moment analysis; hyporheic zone; vertical advective flow

1. Introduction

Flows within sediments near the surface water–groundwater (SW-GW) interface are a controlling factor for hydraulic residence times, chemical fate and transport dynamics, biogeochemical processes, and ecological community structure [1]. This transition zone has been recognized as a major influence on the water budgets and mass balances of solutes within aquatic systems [2,3]. Exchange flows can be challenging to measure accurately due to sediment heterogeneity and the need to integrate measurements at different scales [3,4].

Existing methods to obtain direct measurement of net and cumulative Darcy fluxes within near-surface sediments at the point-scale include the Lee-type seepage meters [5]. They are inexpensive and easy to deploy and errors associated with the method are usually assumed to be insignificant [6]. However, results can be dubious since reliability is difficult to measure [7]. In some cases, repeat measurements have varied by more than 10 times [8], although average cumulative errors have been reported in the range of 66–77 percent of actual flow rates [6,9].

Alternatively, Darcy's law allows estimating local, average, fluxes from measurements of hydraulic conductivity and hydraulic head [8]. This method is universally applicable where these parameters are known however, the method assumes steady-state, one-dimensional flow in homogeneous unconsolidated media. Errors can be introduced when point-measurements of hydraulic conductivity are extrapolated to unmeasured areas. Additionally, hydraulic gradients can be difficult to resolve at low flow rates or at small spatial scales [1].

Heat methods use temperature differences in near-surface sediments to determine flow direction and magnitude [10,11]. Thermal time-series data are analyzed using the Fourier-type heat transport equation (HTE) which accounts for the advective heat transport of the flowing water (convection) and for the conductive heat transport through the material phases of the sediment substrate [5,11]. The HTE is similar to the advection–dispersion equation (ADE) for solute transport. The method

is constrained by initial assumptions including that the interrogated volume be large enough to be described with averaged parameters, and that temperatures at phase boundaries (liquid, solid) are assumed to be equivalent [11]. An inherent liability of heat transport models is their sensitivity to these assumptions [12].

Water budgets provide an overview of a system's hydraulic transport characteristics, comparing inflows and outflows with changes in stored mass for the purpose of determining the temporally and/or spatially-averaged compartmental flow rates [13]. Budgets are often dependent on other measurement techniques for the estimates.

The Sediment Bed Passive Fluxmeter (SBPFM) and Hyporheic Passive Fluxmeter (HPFM) are both point-scale techniques deployed to measure Darcy fluxes and dissolved contaminant fluxes simultaneously, in near-surface sediment exchange zone [4,14]. The two methods are based on the Passive Fluxmeter (PFM) principle [15,16]. The SBPFM measures vertical exchange at the SW-GW sediment interface, while the HPFM measures a vertical profile of distinct horizontal fluxes within the near-surface sediments using isolated sections—similar to the PFM in aquifer well boreholes [15]. The SBPFM and HPFM measure Darcy and dissolved contaminant fluxes using an interior column filled with an activated granular carbon matrix; initially saturated with a suite of alcohol tracers. As water moves through the carbon matrix, tracer mass is eluted in response to the volumetric water flow rate. Following probe retrieval, the remaining tracer and adsorbed contaminant mass are extracted in the lab for analysis.

Here, we introduce the Sediment Bed Borehole Advection Method (SBBAM), which utilizes a push-point probe to quantify the vertical direction and magnitude of Darcy flux at the SW-GW interface. Measurements are derived from residence-time analysis of an introduced tracer calculated from measured tracer concentration time-series data. The SBBAM offers some beneficial design characteristics relative to the current techniques available for measuring SW-GW exchange fluxes in near-surface sediments. The method consists of a direct-push casing acting as an isolated borehole where advective transport within the casing is constrained to the vertical direction removing the effects of horizontal cross-currents seen at the seepage meter chamber opening. Seepage meter bladders also suffer from impingement issues from water-column turbulence which can affect method accuracy. These types of issues are resolved with SBBAM performance because the tracer tests are conducted in protective isolation within the probe interior [5]. Furthermore, the SBBAM provides a direct measure of the flow field, precluding the need for independent estimates of Darcy parameters. Additionally, the SBBAM can provide estimates of mass flux by combining flow rate results and target solute concentration data obtained directly from the flow field using the injection port. The SBBAM does depend on local estimates of vertical and horizontal saturated hydraulic conductivities to define the adjustment factor for flow convergence through the device but can be deployed with much less expense and effort than PFM-based methods. We present results of SBBAM demonstration in the laboratory using a sediment bed simulator tank at eight flow rates ranging from 1 to 90 cm/day.

2. Materials and Methods

2.1. Design

The direct-push casing (Figure 1) consists of a hollow pipe (5 cm ID × 70 cm L) with machined well screen slot sections that are 4 cm long near the top and bottom of the casing. The casing is completely sealed at the top, bottom and lateral boundaries with the exception of the screen intervals, which allow pore-water to flow through the casing, in either direction, depending on local gradients. The central body between the screens acts as a conduit isolating and laterally constraining the vertical component of flow. This central region, with a volume of approximately 730 mL, is the control volume (CV) where the tracer test occurs. The tracer sensor/injection assembly attaches to a removable upper cap that is installed into the casing body after the drive point is inserted into the sediment. Once installed, the upper boundary of the casing is sealed thus allowing flow only in and out of the screen sections.

The skeleton of the internal assembly is built from a 3-D printed fixture made from PLA aliphatic polyester thermoplastic attached to a length of 3/16 in ID steel automotive brake line tubing. The tubing connects to the injection nozzle and extends up through a rubber stopper in the cap. When installed, the fixture is positioned at the midpoint of the CV between the screens. Two conductivity sensors are attached to the fixture with tips positioned at 14 cm equidistant from the injection point and at 2 cm from the screen boundaries within the CV to minimize potential turbulent or complex flow entering and exiting the screens. The use of two sensors provides the ability to determine flow direction in bi-directional systems where the direction is unknown and allows for multiple injection tests during a single deployment to estimate quasi-steady-state flow rates such as experienced in tidally influenced systems with potential for flow reversals. In situations where flow direction is known, such as controlled lab experiments, a single sensor can be employed.

SEDIMENT BED BOREHOLE ADVECTION METHOD

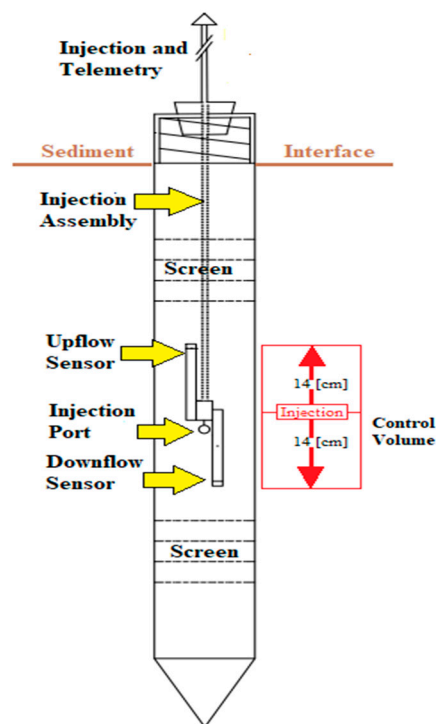


Figure 1. Conceptual design of the SBBAM showing injection and sensor assembly, conceptual control volume, and expected tracer plume path based on bidirectional flow.

2.2. Theory and Operation

The fundamental operating principle of the method relies on temporal moment analysis used to quantify the average travel time of a tracer between the injection port and one of the sensors. For each measurement, 10 mL of NaCl solution is “instantaneously” injected into the assembly, where 3 mL enters the interior of the casing at the center of the CV and the remaining 7 mL occupies excess injection tube capacity for the duration of the test. The tracer concentration is then monitored by a conductivity sensor 14 cm downstream. The term “downstream” refers to the sensor (top or bottom) responsible for measuring instantaneous tracer concentrations and is used here to define the positive direction of advective flow based on local hydraulic gradients. This is important in situations where the interface flow direction is unknown and two sensors are used. In this laboratory tank study, we used a downflow configuration for the experiments where the flow was consistently moving from “surface-to-groundwater”.

Borehole dilution has traditionally been used to estimate horizontal advective velocities in saturated porous subsurface media. For these applications, the average, interior velocities are derived

using the exponential decay behavior of tracer response curves where the CV is continuously mixed. In preliminary work, we found that our tracer responses behaved in a strong plug flow mode (Figure 2) and that estimating velocities using an exponential decay model would have been inappropriate due to the lack of solute mixing. Tracer response curve behavior for the SBBAM is the result of restricted vertical tracer plume movement within the tube CV. The measurably constant flow and low, effective turbulence within the test flow range was seen to consistently create steady response curves from which Darcy velocities are extracted using travel time calculations based on temporal moment analysis.

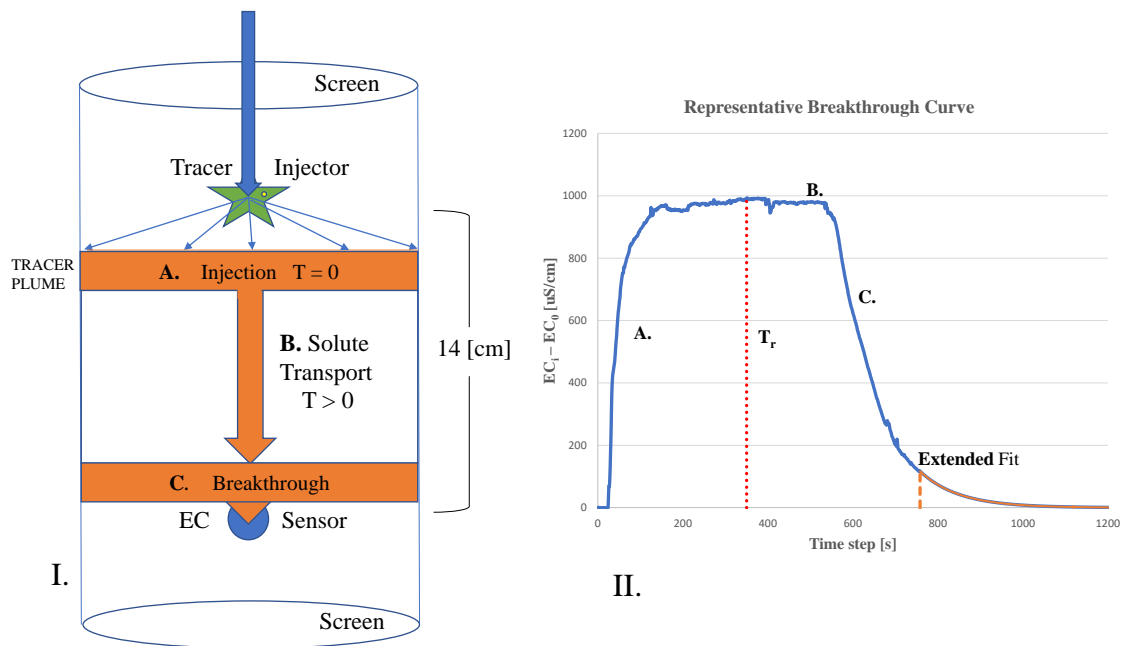


Figure 2. (I) Conceptualization of downward flow Sediment Bed Borehole Advection Method (SBBAM) operation showing the anatomy of observed laminar breakthrough curve (BTC) tracer plume behavior. (II) The three phases of the representative breakthrough curve corresponding to the stages of SBBAM operation with: A. Instantaneous injection, B. Steady-state solute transport, and C. Tracer breakthrough decay. The red and orange dotted lines correspond to an example residence time (T_r) used for Darcy flux calculation and the starting point of the extended fit dataset.

Solute transport processes are described in terms of the flux of solutes into and out of a fixed control volume [17]. The physical processes governing dissolved solute behavior through the control volume are advection and hydrodynamic dispersion due to mechanical mixing and molecular diffusion. Advection defines the average linear bulk velocity (\bar{v}) of a plume’s center of mass. The SBBAM estimates this linear velocity using the tracer concentration breakthrough curve. Not all solute elements are traveling at the plume’s average speed. Hydrodynamic dispersion is a phenomenon of the flow domain causing solute dilution and plume spreading, which does not affect a plume’s mean travel time, however.

Moment analysis is a technique for determining the transport parameters from a travel time distribution function. The n-th moment (M_n) of solute concentration (C) at a downstream location during an infinite time interval is given by

$$M_n = Q \int_0^\infty Ct^n dt, \tag{1}$$

which is the unbounded time-integral of the solute concentration (C) weighted by the time raised to n-th degree. Flow rate Q L/s is assumed to be constant here. Higher degree (i.e., larger n) moments

are often used to characterize complex flow, but for this study, we are only concerned with the zeroth and first moments, which represent the area under the concentration–time curve and relate to the mean tracer arrival time, respectively. Since our datasets consist of discrete data, the general form is modified to

$$M_0 = Q \sum_i C_i \Delta t, \quad (2)$$

$$M_1 = Q \sum_i C_i t_i \Delta t, \quad (3)$$

Here, M_0 mg (2) represents the total injected mass in the system and C_i mg/L are the instantaneous concentrations measured at times t_i s separated by steps of $\Delta t = 1.0$ s during our experiments. The center of mass (centroid) of the BTC represents the average residence time (T_r) of the tracer [18] (4).

$$T_r = M_1/M_0, \quad (4)$$

The Darcy flux (q_c) of the plume centroid inside the CV is equal to the linear velocity and estimated using the residence time and plume travel distance $D = 14$ cm (5).

$$q_c = D/T_r, \quad (5)$$

Once an estimate of q_c is determined within the casing using Equation (5), an adjustment factor is necessary to relate the measured flow within the borehole casing (q_c) to actual and undisturbed flow (q_0) within the surrounding sediment (7). The adjustment is required because of the contrast between open-pipe flow hydraulic conductivity (K_c) within the casing and the hydraulic conductivity within the ambient sediment (K_{sed}). The fact that $K_c \gg K_{sed}$ creates a convergent preferential flow path through the probe resulting in measured fluxes that are larger than in the undisturbed surrounding sediment. This convergence behavior is a well-known aspect of techniques that estimate flows using internal control volumes embedded within a porous media, such as a well-casing [19] and the well screens containing the Passive Flux Meter (PFM) [15,16]. Although flow field geometry is non-linear in all of these applications, the deviation between internally measured and actual ambient subsurface flows can be simplified to a linear relationship and accounted for using a constant of proportionality (F_0), Equation (6).

$$q_0 = q_c/F_0, \quad (6)$$

The flow convergence factor F_0 depends on the geometry of the SBBAM casing and the hydraulic conductivities K_h and K_v of the sand in the horizontal and vertical directions, respectively. The factor is quantified based on existing work for the SBPFM [4,20], knowing that the hydraulic conductivity K_c of the open casing (i.e., no sorbent medium) between both SBBAM screens is very much larger than both K_h and K_v . First, $K_v = 31.8$ m/day was determined from two falling head conductivity tests through an impermeable pipe casing inserted into the sand to the depths of each screen [4] (p. 4). Next, $\rho = 0.65$ was found from injecting water simultaneously through both SBBAM screens, observing steady-state injection flow rate and head of 0.23 m³/day and 0.6 cm, respectively, and applying $Q_{inj}/(aK_v \phi_{inj}) = 40$, with the understanding that the geometric configurations of the SBPFM and SBBAM are approximately the same. Finally, we estimated $F_0 = 55$ from [4] (p. 4), where $\log_{10}[s/(\rho a)] = 0.45$ and $p/s = 6.7$.

2.3. Sand Tank Experimental Design

The SBBAM device was tested in a sand-filled, constant head, simulator (Figure 3, Table 1). The simulator consisted of two 55-gallon polymer drums. One drum served as the sediment simulator and was filled with sand into which the probe body was embedded.

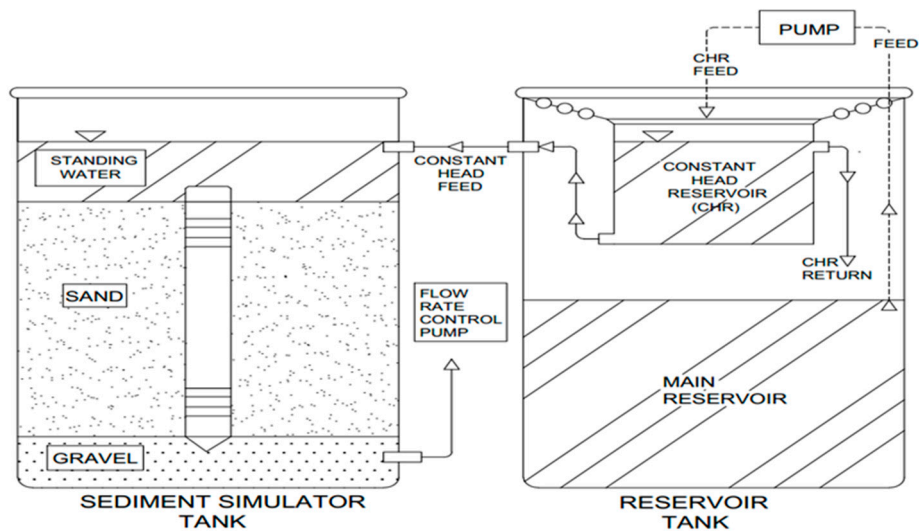


Figure 3. Sediment simulator tank with probe body and main reservoir with constant head reservoir tank.

Table 1. Catalogue of dimensions for the Sediment Simulator, Reservoir Tanks and SBBAM Casing.

TANK	Units	
Volume	m ³ /day	0.21
Height	m	0.9
Diameter	m	0.58
Area	m ²	0.264
Gravel Layer	m	0.1
Sand Layer	m	0.54
Standing Water	m	0.17
SBBAM CASING		
Total Length	cm	69.5
Outer Dia. (OD) (a)	cm	6
Inner Dia. (ID) (r)	cm	5
Screen Length (s)	cm	5.4
Distance b/w Screens (p)	cm	36.5

The drum contained bulkhead fittings near the top and bottom to allow the entrance and exit of water while maintaining a constant head boundary of approximately 17 cm above the sediment interface. Flow direction through the tank was determined by the configuration of the pump.

Downward flow was initiated by pumping from the bottom of the tank; upward flow from the top. Downward flow was the primary test configuration used in this study. Limited tests for upward flow were conducted to verify that the lower sensor showed no signal during dual-sensor operation. The second drum served as a reservoir to maintain a constant head in the sediment simulator. The reservoir consists of the main 55-gallon (0.21 m³) reservoir for primary storage and a smaller, 5-gallon bucket which was suspended to a height that the head maintained within the bucket would regulate the head within the sediment simulator (Figure 3).

The sediment simulator was filled with pea gravel and medium-to-fine, commercial-grade sand. Pea gravel was packed to a height of 10 cm thick from the bottom of the tank, covering the bulkhead port. This protected the bottom port from sand intrusion. A thin, permeable, mesh was placed between the gravel and sand layer to minimize intermixing, after which the probe body was placed on the gravel layer in the radial center of the tank as sand was wet-packed to a thickness of 54 cm by alternately adding water and sand until the upper screen of the probe was covered by a few centimeters. The wet-pack method minimized trapped air within the sand layer. Additional water was added until

the elevation head at the upper inlet reached 17 cm above the sand interface. This level was maintained at a steady-state by the constant head reservoir for the duration of the tests.

We anticipate that the current blunt-force method of drive-point deployment could modify the hydraulic conditions in local sediments at a field site during installation. Another method, where a removable drive-sleeve is first inserted and the interior sediment core removed prior to SBBAM probe installation, could be utilized to minimize this disturbance [14].

2.4. Simulator Media

Sieve test analysis was performed on ten 0.5 kg samples of sand to verify that the particle size distribution fit the stated characteristics of the commercial product. The particle size distribution showed that the 10th, 60th and 90th percentiles of grain-size diameter were $d_{10} = 0.17$ mm, $d_{60} = 0.355$ and $d_{90} = 0.50$ mm confirming that ninety percent of samples were within the range of grain-size diameters (0.05–0.5 mm) indicated for medium to fine, well-sorted sand. The uniformity coefficient for the sand ($UC = d_{60}/d_{10}$) was 2.1.

2.5. Test Protocol

The lab tests were run at 8 flowrates, {2, 8, 25, 50, 75, 100, 125, 153} mL/min, representing 8 specific discharges {1, 5, 15, 29, 44, 74, 90} cm/day through the tank. Three or four trials were performed at each flowrate.

Each test followed a consistent protocol. Flowrates through the tank were set at the pump and verified with probe screens closed. Sensor operation and datalogging equipment were initiated to verify microprocessor serial port operation and SD flash memory initiation. Next, 40 mL of pore-water (2 syringe volumes) was removed via the injection port prior to each test to verify background concentrations and sensor operation at the serial monitor and to flush the injection tube of tracer solution from previous tests. Tracer solutions were injected into the injection port by affixing the syringe, opening the port valve, emptying syringe contents within 3 s, and closing the valve. Data points were counted on the monitor between the injection time and initial sensing above background. This lag was used to subtract out pre-injection data points from the dataset and ranged between 5–15 data points.

2.6. Tracer Concentration and Volume

Tracer solutions were prepared by weighing out 58.44 g of laboratory-grade (Fisher S-271) NaCl, on a scale and diluted with DI water in a 1 L volumetric flask. Solutions were kept well-mixed using a magnetic stirring plate. Small volumes of <50 mL were transferred to a covered 100 mL beaker for syringe loading of individual tests.

Tracer solution volume was determined from a series of tests run at 15, 29, 59, and 90 cm/day with a 1.0 M NaCl solution. All four flowrates were tested at volumes of both {2, 3} mL. Tracer solution volume was then increased to 4, 5, and 6 mL for rates 29, 59, and 90 cm/day. The tests showed reasonable precision and accuracy at all solution volumes tested with correlation coefficients between $0.9961 \leq r \leq 0.9996$. We settled on 3 mL which had the best results across all flowrates ($r = 0.9996$) for the duration of the tests, including the lowest flowrates {1, 5} cm/day which were run during an independent set of tests. Preliminary trials indicated that, while variations in tracer injection volume did affect concentration readings by increasing the total mass of the system, injection volume was not seen as a significant parameter affecting SBBAM results during these trials.

Due to injection tube assembly containing 7 mL of empty capacity, 10 mL of solution was injected to ensure the 3 mL entered the CV, with the remaining solution vacuum-stored in the tube and removed after test termination.

2.7. Data Collection

All components used for data collection, transfer, and storage are based on Arduino and Arduino compatible technology. Arduino technology is an inexpensive, open-source electronic and software

prototyping environment. Electrical conductivity (EC) data were collected using an Atlas Scientific K1.0 conductivity sensor at 1.0 s^{-1} intervals and sent, via UART protocols, to an Arduino Uno R3 microcontroller which relayed the signal to a laptop serial monitor interface for real-time observation, and to an SD flash memory card for storage.

The heart of the data collection system is the Arduino Uno REV3 microcontroller. Signal data were stored in flash memory using an SD datalogging shield from Adafruit. The K1.0 conductivity sensor measures values between $5\text{--}200\text{ K }\mu\text{S/cm} \pm 2\%$ (Atlas Scientific, Long Island, NY, USA). The current experiments operated between $300\text{--}2500\text{ }\mu\text{S/cm}$. Sensor error is expected to be $<1\%$ within the operating range of these experiments. The EC sensor was calibrated using a 2-point calibration provided by the manufacturer. The use of tap water in the tank resulted in an average background concentration of $300\text{ }\mu\text{S/cm}$.

Preconfigured code for shield and sensor interface were obtained from the manufacturers, Arduino IDE libraries, and outside sources. The code was then modified to fit the current experiment.

3. Results

All test results presented (Figure 4, Table 2) here are for flow in the downward direction where the bottom sensor was consistently used. The process under upward flow conditions was evaluated using the upper sensor and reversing the flow in the tank. Tests run in the upward flow direction confirmed that no tracer solution was observed at the bottom sensor, not even at the lowest rates. Further testing for dynamic bi-directional usage is warranted.

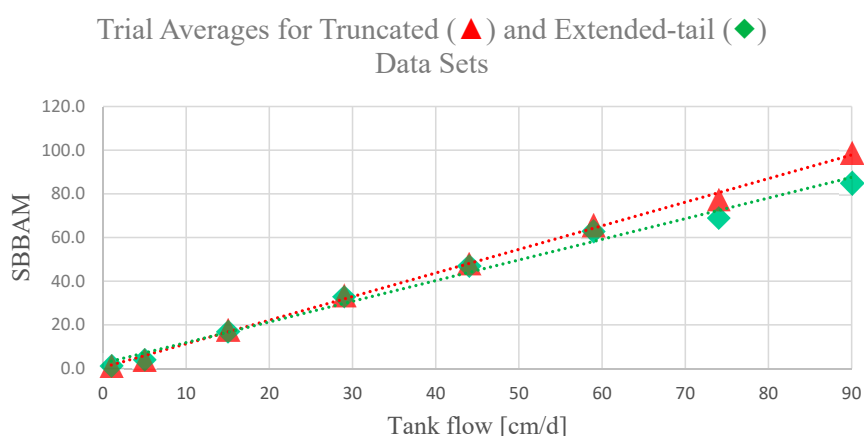


Figure 4. A comparison of calculated averages for truncated and extended-tail Darcy flux measurements for the eight flowrates investigated. The values are derived from BTC curves using $F_0 = 55$. Red triangles show original truncated test averages $-R^2 = 0.9977$. Green diamonds show extended-tail results $-R^2 = 0.9893$.

Table 2. Sample statistics, % error w/1-STD for each flow rate, and 95th percentile confidence intervals with upper (UB) and lower (LB) boundaries for regular trials (columns 1–5). Results adjusted for the effects of asymptotic tailing, and percent difference b/w truncated and extended BTCs (columns 6–7), * indicates the lower tests were run to background, - indicates no data.

Nominal cm/day	$\bar{x} \pm s$ cm/day	Error ± 1 -STD (%)	Two-Tail 95% Confidence Interval		Extended-Tail Adj cm/day	% Diff (%)
			UB (+)	LB (-)		
1	1.2 ± 0.4	20 ± 30	1.8	0.6	*	-
5	4.3 ± 1.3	14 ± 30	6.3	2.3	*	-
15	18 ± 3.0	19 ± 20	22.7	13.1	17 ± 3	-5
29	34 ± 3.5	16 ± 12	39.2	28	33 ± 3.6	-2
44	48 ± 2.3	9 ± 5	53.8	42.4	47 ± 3.6	-2
59	66 ± 4.4	11 ± 7	76.5	54.7	63 ± 2.7	-3
74	77 ± 5.4	4.6 ± 7	86	68.8	70 ± 3.9	-11
90	99 ± 9.0	10 ± 10	113.3	84.7	85 ± 2.9	-14

Descriptive sample statistics (Table 2) of individual trials were calculated along with percent error and percent deviation. The student-t method was used to estimate two-tailed 95% confidence intervals. The results of the breakthrough curves (BTC) consistently showed predominantly plug flow tracer plumes (Table 2). Laminar flow within the bore-hole casing was strongly suggested by both the breakthrough curve shapes and Reynolds' numbers derived from calculated interior velocities ($Re < 100$ for all tests). The derived open-flow factor of $F_0 = 55$ returned average errors between 4–20% for the breakthrough curve evaluations. There was an observable negative trend regarding percent error increasing with decreasing flow rate. The range considered in this study lead to a good match between measured and applied Darcy flux with a higher relative error at the lowest flux considered. This suggests that the Darcy flux detection limit for the approach might be between 1 and 5 cm/day. Note however that some aspects of the design could be modified such as probe diameter and distance between screen section to lower the detection limit.

4. Discussion

When considering the quality of the experimental results, one should be aware of the empirical nature of the data, representing controlled parameters in a laboratory environment. For future field applications where many site parameters are either unknown or must be inferred, a firm understanding of the potential errors inherent to the SBBAM is important.

The resultant fit of the lab study showed high linearity ($r^2 = 0.9977$) (Figure 4, Table 2) and relatively low cumulative error. This suggests that the errors inherent in different aspects of this method can be managed effectively in a controlled environment. The main areas of potential error include tracer mass recovery, plume-centroid location assumptions, discrepancies with data collection, and errors in calculating F_0 . The study results suggest that we were able to minimize the cumulative effects of these errors, however, a brief discussion of some potentially confounding issues should be illuminating for future trials.

Cumulative sensor operation and data collection errors were minimal. Potential errors associated with the shape factor (F_0), which are primarily related to incorrect estimates of site hydraulic conductivity and anisotropy, are addressed fully in Layton et al. (2017) [4]. Small errors in characterizing hydraulic conductivity affect the shape factor by approximately 10% for every 10% discrepancy between vertical and horizontal conductivities. However, as mischaracterizations grow larger than 50%, shape factor error begins to increase due to the nonlinear nature of the method.

Because of the skewed nature of the tracer age distributions which are often characterized by long-term asymptotic tailing, tests were terminated before background concentrations were reached; typically, within 200 $\mu\text{S}/\text{cm}$ (Figure 2). This results in an underestimation of residence times and overestimation of fluxes due to the mathematical artifacts of the moment analysis. To assess the error associated with prematurely terminating the BTCs, we extended them toward background concentrations, below 0.1 $\mu\text{S}/\text{cm}$, and recalculated results. Extended tailings were created by extrapolating truncated tails using an exponential fit of the dataset [18].

Based on the analysis, the effects of premature termination are ≤ 5 percent for {15–59} cm/day. A positive trend is evident, showing increased deviation as flow rates increase. The disparity associated with truncated and extended tails is exacerbated at the highest flow rates, {74, 90} cm/day. A positive correlation suggests that, at lower flow rates, plug flow conditions contribute to higher tracer mass recovery at breakthrough. The lack of mass recovery at the higher rates is likely due to increased mixing leading to longitudinal spreading of the tracer plume. This was originally discussed for continuous flow reactors [21]. Overall, however, the initial truncated method has a better linear fit ($r^2 = 0.9977$) compared to the extended fit ($r^2 = 0.9893$).

Tracer plume transit distance can introduce systemic error into the apparent velocity calculation (5) due to the effect of initial plume spreading on injection. The SBBAM relies on a fixed distance between the sensor and injection point to determine the velocity and assumes that the injected tracer plume centroid is located at the injection point. In reality, the plume centroid is likely longitudinally offset

due to turbulence upon injection. Percent errors related to injection-point variability are cumulatively linear, introducing about 7.0% error per 1 cm deviation in sensor distance. These errors are expected to be more pronounced as flow rates increase due to increased turbulence and longitudinal mechanical spreading within the column. If proper procedures are applied, tracer plume distance error is not expected to be more than a few centimeters and can be easily calibrated with the adjustable sensor.

The next set of experiments should focus on a field application of the SBBAM. The method could be deployed in a controlled environment, such as a constructed wetland cell or infiltration basin, where infiltration rates could be readily confirmed from available hydrological data. In addition, other methods, such as seepage meters, could be concurrently deployed alongside each SBBAM probe for comparison. Accurate characterization of site sediment hydraulic conductivities would be necessary to correctly estimate the shape factor (F_0).

5. Conclusions

In conclusion, the Sediment Bed Borehole Advection Method was found to be relatively easy to employ once the initial setup was achieved and through the use of an automated spreadsheet returned a quick estimate of the Darcy flux within the column. Overall, the precision of the BTCs demonstrated the replicability of the method, and the agreement between measured rates and expected values validates the method used for determining the open-flow shape factor under controlled conditions (Figure 4).

Author Contributions: Conceptualization, H.K. and M.D.A.; methodology, S.A. and J.C.; formal analysis, S.A. and K.H.; writing, S.A. and M.D.A. All authors have read and agreed to the published version of the manuscript.

Funding: This research was funded by a grant from Occidental Chemical (OXYCHEM), grant number AWD01957.

Conflicts of Interest: The authors declare no conflict of interest. The funders had no role in the design of the study; in the collection, analyses, or interpretation of data; in the writing of the manuscript, or in the decision to publish the results.

References

1. Krause, S.; Hannah, D.M.; Fleckenstein, J.H.; Heppell, C.M.; Kaeser, D.; Pickup, R.W.; Pinay, G.; Robertson, A.L.; Wood, P.J. Inter-disciplinary perspectives on processes in the hyporheic zone. *Ecohydrology* **2011**, *4*, 481–499. [[CrossRef](#)]
2. Winter, T.; Harvey, J.; Franke, O.; Alley, W. Groundwater and Surface Water: A Single Resource. In *Circular*; U.S. Geological Survey: Reston, VA, USA, 1999; p. 1139.
3. Sophocleous, M. Interactions between groundwater and surface water: The state of the science. *Hydrogeol. J.* **2002**, *10*, 52–67. [[CrossRef](#)]
4. Layton, L.; Klammler, H.; Hatfield, K.; Cho, J.; Newman, M.; Annable, M.D. Development of a passive sensor for measuring vertical cumulative water and solute mass fluxes in lake sediments and streambeds. *Adv. Water Resour.* **2017**, *105*, 1–12. [[CrossRef](#)]
5. Brodie, R.S.; Baskaran, S.; Ransley, T.; Spring, J. Seepage meter: Progressing a simple method of directly measuring water flow between surface water and groundwater systems. *Aust. J. Earth Sci.* **2009**, *56*, 3–11. [[CrossRef](#)]
6. Belanger, T.V.; Montgomery, M.T. Seepage meter errors. *Limnol. Oceanogr.* **1992**, *37*, 1787–1795. [[CrossRef](#)]
7. Kaleris, V. Quantifying the exchange rate between groundwater and small streams. *J. Hydraul. Res.* **1998**, *36*, 913–932. [[CrossRef](#)]
8. Murdoch, L.C.; Kelly, S.E. Factors affecting the performance of conventional seepage meters. *Water Resour. Res.* **2003**, *39*, 1163. [[CrossRef](#)]
9. Kennedy, C.D.; Murdoch, L.C.; Genereux, D.P.; Corbett, D.R.; Stone, K.; Pham, P.; Mitsova, H. Comparison of Darcian flux calculations and seepage meter measurements in a sandy streambed in North Carolina, United States. *Water Resour. Res.* **2010**, *46*. [[CrossRef](#)]
10. Rau, G.C.; Andersen, M.S.; McCallum, A.M.; Roshan, H.; Acworth, R.I. Heat as a tracer to quantify water flow in near-surface sediments. *Earth-Sci. Rev.* **2014**, *129*, 40–58. [[CrossRef](#)]
11. Silliman, S.E.; Booth, D.F. Analysis of time-series measurements of sediment temperature for identification of gaining vs. losing portions of Juday Creek, Indiana. *J. Hydrol.* **1993**, *146*, 131–148. [[CrossRef](#)]

12. Rudnick, S.; Lewandowski, J.; Nutzmann, G. Estimation of lacustrine groundwater discharge using heat as a tracer and vertical hydraulic gradients—A comparison. *Proc. Int. Assoc. Hydrol. Sci.* **2015**, *365*, 79–84. [[CrossRef](#)]
13. Healy, R.W.; Winter, T.C.; LaBaugh, J.W.; Franke, O.L. Water Budgets: Foundations for Effective Water-Resources and Environmental Management. In *Circular*; US Geological Survey: Reston, VA, USA, 2007.
14. Kunz, J.V.; Annable, M.D.; Cho, J.; Von Tümpling, W.; Hatfield, K.; Rao, S.; Borchardt, D.; Rode, M. Quantifying nutrient fluxes with a new hyporheic passive flux meter (HPFM). *Biogeosciences* **2017**, *14*, 631–649. [[CrossRef](#)]
15. Hatfield, K.; Annable, M.; Cho, J.; Rao, P.S.C.; Klammler, H. A direct passive method for measuring water and contaminant fluxes in porous media. *J. Contam. Hydrol.* **2004**, *75*, 155–181. [[CrossRef](#)]
16. Annable, M.D.; Hatfield, K.; Cho, J.; Klammler, H.; Parker, B.L.; Cherry, J.A.; Rao, P.S.C. Field-Scale Evaluation of the Passive Flux Meter for Simultaneous Measurement of Groundwater and Contaminant Fluxes. *Environ. Sci. Technol.* **2005**, *39*, 7194–7201. [[CrossRef](#)]
17. Freeze, R.; Cherry, J. *Groundwater*; Prentice-Hall: Englewood Cliffs, NJ, USA, 1979.
18. Shook, G. A systematic method for tracer test analysis: An example using Beowawe tracer data. In Proceedings of the Thirtieth Workshop on Geothermal Reservoir Engineering, Stanford University, Stanford, CA, USA, 31 January–2 February 2005.
19. Drost, W.; Klotz, D.; Koch, A.; Moser, H.; Neumaier, F.; Rauert, W. Point dilution methods of investigating ground water flow by means of radioisotopes. *Water Resour. Res.* **1968**, *4*, 125–146. [[CrossRef](#)]
20. Klammler, H.; Hatfield, K.; Nemer, B.; Mathias, S.A. A trigonometric interpolation approach to mixed-type boundary problems associated with permeameter shape factors. *Water Resour. Res.* **2011**, *47*, 03510. [[CrossRef](#)]
21. Danckwerts, P. Continuous flow systems. Distribution of residence times. *Chem. Eng. Sci.* **1953**, *2*, 1–13. [[CrossRef](#)]

Publisher's Note: MDPI stays neutral with regard to jurisdictional claims in published maps and institutional affiliations.



© 2020 by the authors. Licensee MDPI, Basel, Switzerland. This article is an open access article distributed under the terms and conditions of the Creative Commons Attribution (CC BY) license (<http://creativecommons.org/licenses/by/4.0/>).